The Visual Computer
https://doi.org/10.1007/s00371-023-02964-1

ORIGINAL ARTICLE

# A mixed reality framework for microsurgery simulation with visual-tactile perception

Nan Xiang[1] · Hai-Ning Liang[1] · Lingyun Yu[1] · Xiaosong Yang[2] · Jian J. Zhang[2]

Accepted: 9 June 2023


**Abstract**
Microsurgery is a general term for surgery combining surgical microscope and specialized precision instruments during operation. Training in microsurgery requires considerable time and training resources. With the rapid development of computer technologies, virtual surgery simulation has gained extensive attention over the past decades. In this work, we take advantage of mixed reality (MR) that creates an interactive environment where physical and digital objects coexist, and present an MR framework for the microsurgery simulation. It enables users to practice anastomosis skills with real microsurgical instruments rather than additional haptic feedback devices that are typically used in virtual reality-based systems, and to view a realistic rendering intra-operative scene at the same time, thus creating an immersive training experience with such a visual-tactile interactive environment. A vision-based tracking system is proposed to simultaneously track microsurgical instruments and artificial blood vessels, and a learning-based anatomical modeling approach is introduced to facilitate the development of simulations in different microsurgical specialities by rapidly creating virtual assets. Moreover, we build a prototype system for the simulation specializing in microvascular hepatic artery reconstruction to demonstrate the feasibility and applicability of our framework.

**Keywords** Virtual surgery · Mixed reality · 3D tracking · 3D modeling

## 1 Introduction

Microsurgery is a surgical subdiscipline that combines magnification with surgical microscopes, specialized precision tools and anastomosis techniques (see Fig. 1) [1, 2]. Microanastomosis techniques are primarily used to anastomose micro blood vessels and nerves, which are widely utilized in modern surgical operations such as plastic surgery, transplant surgery, ophthalmic surgery, and artery reconstruction [1, 3]. However, a qualified microsurgeon requires a very long learning curve to gain adequate anastomosis skills [3]. According to the types of the materials used in the training process, the traditional training models can be classified into two main categories: *synthetic* model and *biological* model [4–7]. As illustrated in Fig. 1, the synthetic models, also known as non-living models, are made from artificial materials [4, 5]. They are cost-effective, but lack of realism from the visual sense [4, 5]. The biological models refer to animal cadaveric tissues and live animals, which have been considered as the "gold standard" of microsurgical training [8]. However, the biological models always face the issues related to the ethical treatment of animals and incur high costs in a long-term usage [4–6, 8]. With advances in computing technologies, especially in computer-aided simulation, surgical training is undergoing a rapid evolution. Virtual surgery simulation provides a visually plausible, non-hazardous and effective supplement to the traditional microsurgical training.

The virtual reality (VR)-based system typically combines a head-mounted display (HMD) and 1–2 haptic feedback

✉ Nan Xiang
Nan.Xiang@xjtlu.edu.cn

✉ Xiaosong Yang
xyang@bournemouth.ac.uk

Hai-Ning Liang
HaiNing.Liang@xjtlu.edu.cn

Lingyun Yu
Lingyun.Yu@xjtlu.edu.cn

Jian J. Zhang
jzhang@bournemouth.ac.uk

[1] Department of Computing, School of Advanced Technology, Xi'an Jiaotong-Liverpool University, Suzhou, China

[2] National Centre for Computer Animation, Bournemouth University, Poole, UK

Published online: 30 June 2023

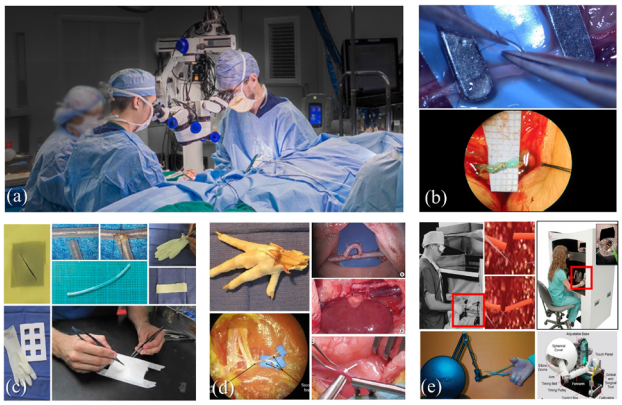

**Fig. 1** **a** Microsurgery operating room [2]. **b** Intra-operative views under the surgical microscope. **c** Practice Card and Gauze & Tape models [9]. **d** Animal models include chicken, rat and rabbit [8, 10]. **e** Virtual microsurgery simulators with modified haptic feedback devices [11, 12]

devices (HFDs) [13]. The HFD provides the force feedback and the interaction means while the HMD presents the visual rendering result of the intra-operative scene to the users. This combination has also been applied to the microsurgery simulation. However, though some studies have made efforts to modify the HFD to make it more usable for the microsurgery simulation (see Fig. 1e), its interaction pattern does not seem to fit very well with microsurgery, and the simulated force generated by the HFD cannot provide users with the surgical tactile force from the fingertip which is one of the most essential factors in microsurgical training [4, 13]. Compared with VR-based systems that put users in a fully digital world, mixed reality (MR) creates an interactive environment where physical and digital objects coexist, which is likely to be a more promising alternative for microsurgery simulation. In this research, we propose an MR framework for the microsurgery simulation that leverages the affordances of MR technologies. It allows users to practice on physical objects (artificial blood vessels made by soft silicone tubes) and use real microsurgical instruments rather than additional devices. As shown in Fig. 2, the motion and deformation data are captured for the simulation procedure via a vision-based system, which are then applied to drive the corresponding digital objects move. The realistic rendering intra-operative view of microsurgery is presented onto the lens of an HMD. In this scenario, the HMD can be considered as an effective substitute for the surgical microscope. In addition, a learning-based method is proposed to rapidly reconstruct 3D models from single 2D X-ray images, which can greatly facilitate the development of simulations for different microsurgical specialities.

A couple of challenges include interaction design, accurate tracking and efficient 3D modeling need to be overcome to make the blueprint into reality. Both hardware design and software development are involved in this project. The difficulty of the design lies in finding ways of simulating an interactive environment which provides users experiences as natural as that of surgeon operating microsurgical instruments during a real microsurgery. After a few microsurgical observations and communicating with a senior microsurgeon, we propose a metal workbench-centered hardware design as shown in Fig. 2. In addition, an effective tracking approach that can simultaneously capture the motion of microsurgical instruments and the deformation of artificial blood vessels is crucial to this project. Among various tracking approaches, the vision-based method is considered as a promising candidate for the tracking of surgical instruments because it is contactless sensing, light weight and cost-effective [14]. Besides, the captured images not only can be used for tracking but also can be used for compositing MR images, which makes visual sensing a perfect fit for this MR-based simulation. However, there is few vision-based method to the best of our knowledge can simultaneously track multiple rigid objects and deformable objects in the virtual surgery. We employ several 3D printed platonic markers [15] along with a modified statistical method to track the microsurgical instruments, propose an efficient hybrid algorithm for the tracking of artificial blood vessels, both of which are integrated into a multi-view tracking system. As for the anatomical modeling, the patient-specific modeling (PSM) that reconstructs anatomical models from patient-specific data [16] provides a source of inspiration for our work. Compared with the traditional PSM work that usually reconstructs models with *voxel* or *point cloud* format from 3D volumetric imaging data [16–18], we present a learning architecture that generates *3D mesh* organ models directly from single 2D X-ray images.

In simple terms, the main contributions of this work can be summarized as:

- An MR framework for microsurgery simulation is presented. It aims to increase the immersion by providing users with a visual-tactile interactive experience. Both the hardware and software are developed in this work.
- A series of essential techniques are presented. They constitute the main functional modules of our framework, including vision-based surgical instruments tracking, artificial blood vessels tracking, and learning-based anatomical 3D modeling.

## 2 Related work

### 2.1 Microsurgery simulation

Simulation-based methods are popular in microsurgical training and incorporated into the standard practical training courses. Various simulators have been proposed, which

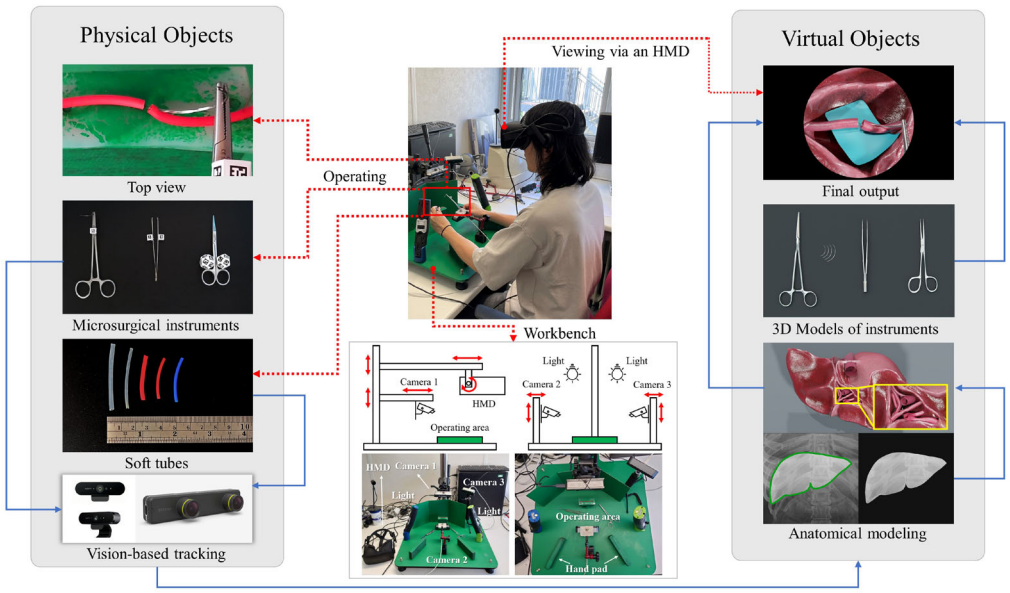


**Fig. 2** Framework overview

can be classified into three main categories according to the model types: *synthetic* models, *biological* models, and *virtual* models [4–7]. The *Synthetic* models refer to the artificial materials which are used to simulate real soft tissues. Fanua et al. [19] use a practice card which is made of surgical gloves and medical grade tubes to substitute for the laboratory animals in the microsurgical training. A course of microsurgery essentials released by Stanford University School of Medicine [9] suggests a practice card and a tape model made from latex surgical gloves (Fig. 1c). Polyvinyl alcohol (PVA) gelatin tubes and silicone tubes are employed in some simulators for anastomosis training [20, 21]. To give it a more realistic simulation, a PVC-rat anatomical model is introduced [22]. Similarly, De Virgilio et al. [23] build a human-size silicone mannequin model in their microsurgical exercise platform.

Although synthetic models allow users to practice on the physical soft materials in an efficient and cost-effective way, they cannot fully substitute the biological models due to the lack of visual fidelity [4, 7]. As shown in Fig. 1d, rabbit, rat, chicken and their tissues are the most commonly used biological models [4]. In the Stanford's microsurgery essentials course [9], chicken feet are utilized as high fidelity models for microvascular anastomosis training. Chicken thighs are also frequently used in practice [24, 25]. Compared with the single organ models, live animals are identified as the best substrates for the training of microsurgical techniques because of the presence of natural "wet" environment [5, 10, 26, 27], which is the "gold standard" for the microsurgery simulation despite ethical issues and high costs [7]. For instance, New Zealand albino rabbits are employed by de Giacomo Carneiro et al. [26] and Wanderer et al. [10] for anastomosis training. Rodríguez et al. [28] and Yamamoto et al. [27] choose live rats as the substrate in their training simulators.

Advances in computer-aided technologies have led to a growing interest in virtual microsurgery simulators. A VR-based microsurgery simulator is introduced by O'toole et al. [29] as early as 1999. It shows virtual models have a positive impact on anastomosis training, similar conclusions are drawn by Kazemi et al. [30] and Alaraj et al. [31]. Although the virtual microsurgery simulators have been explored for decades, the interaction pattern and the combination of HMD and HFD have barely changed. Some recent studies focus on modifying HFDs to enhance the fidelity of the devices. Hoshyarmanesh et al. [12] propose a microsurgery-specific haptic device with articulated structure as shown in Fig. 1e. However, the simulated force is no substitute for the real force from the microsurgical instruments (e.g., forceps, needles, and scissors.) after all. Our framework aims to create an MR-based interactive environment that allows users to feel realistic force feedback from their fingertips, and meanwhile provides a visually plausible experience.

## 2.2 Vision-based tracking for surgical instruments and soft tissues

Vision-based tracking of surgical instruments has permeated into various surgical specialities, such as endoscopic surgery, cholecystectomy, and neurosurgery. Ryu et al. [32] present a hybrid vision algorithm combining k-means classification and Kalman filter tuning for tracking a robot arm in a robot-assisted endoscopic surgery. Yang et al. [33] introduce a self-contained tracking framework via ultrasound image-based localization to register the initial camera position with

its scene geometry. Sánchez-González et al. [34] present a method for laparoscopic instrument tracking via image segmentation accompany with 3D reconstructed abdominal structures. Robu et al. [35] propose a geometric object descriptor to help with overlapping bounding box disambiguation, which achieves promising accuracy in tracking laparoscopic tools. There are some research projects use fiducial markers to improve the robustness and accuracy. A tracker comprised of a set of squared markers and an electromagnetic sensor is introduced by Liu et al. [36] to track the motion of a laparoscopic ultrasound transducer. Gadwe et al. [37] present a cylindrical handle with a series of squared markers wrapped, for the tracking of cylindrical surgical instruments. However, these methods are mostly stuck with estimating a single pose for a single instrument in a specific scenario, cannot be directly applied to track multiple microsurgical instruments.

Vision-based methods have also been applied to track soft tissues. Richa et al. [38] present a thin-plate spline deformable model to track the beating heart surface from stereo images. Wong et al. [39] also propose a deformable model for soft tissues tracking, which is based on a quasi-spherical triangle surface. A matching-based method is introduced by Yang et al. [40]; it consists of two recursive processes, a kernel-based inter-frame motion estimation and a model-based intra-frame 3D matching algorithm. Under a stereo microscopic view, Schoob et al. [41] present a linear parametrization method enabling left-right consistency for stereoscopic tracking of the soft tissues motion. Song et al. [42] propose a warping field based on embedded deformation nodes, which allows it to capture the deformation data of surfaces incrementally. In this work, we present a vision-based system that is able to simultaneously estimate six-degrees-of-freedom (6DoF) poses and capture deformation data for the MR-based microsurgery simulation.

### 2.3 Patient-specific anatomical modeling

Research on patient-specific anatomical modeling has increased tremendously over the past decades. Different organs and anatomical structures can be reconstructed from patient-specific data. The process typically can be divided into five steps: (1) *patient-specific data acquisition*, (2) *medical image segmentation and registration*, (3) *3D model generation*, (4) *material properties assignment*, and (5) *simulation test* [16, 17, 43]. The most commonly used patient-specific data are derived from MRI, CT, ultrasound and X-ray images, which have become the main source for anatomical modeling [16–18, 44].

With recent progress in utilizing deep neural networks (DNNs) for image segmentation and 3D shape acquisition, there has been a great increase in introducing DNNs into the anatomical modeling pipeline. A computationally efficient

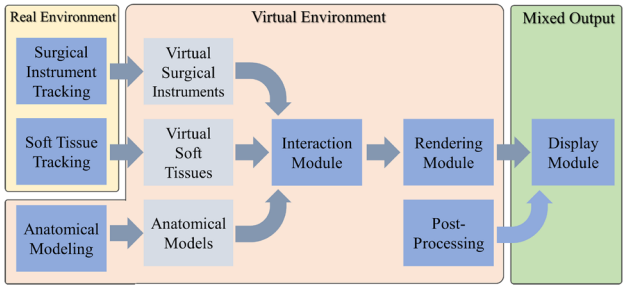


**Fig. 3** The system pipeline and data flow. The blue boxes represent the main functional modules, and the grey boxes denote the output data. Arrows indicate the directions of the data flows

modeling framework is presented by Tahir et al. [45]; this learning-based approach is used for brain vascular segmentation. DeepSSM [46] is a framework that contains CNNs to extract 3D shapes with a low-dimensional representation from 3D imaging data. Kong et al. [47] claim a hybrid network architecture to predict the 3D shape of a heart from 3D volumetric CT and MR images. Each approach mentioned above focuses on one step of PSM or reconstructing a specific anatomical structure. We present an end-to-end learning architecture that is capable of generating 3D mesh from a single 2D image. The generated mesh can be directly used to build virtual environments for the microsurgery simulations.

## 3 Framework overview

The framework can be divided into hardware and software parts. A workbench is designed and manufactured to wrap the devices and instruments in a compact workspace as shown in Fig. 2. It is made of iron and steel; the main body is an iron plate with a steel column standing on top of it. The essential components including an HMD (Oculus Rift), cameras (two Logitech webcams and a ZED mini stereo camera), lights, operating area and hand pads are attached to the base plate via industrial magnets. A magnetic arm system is employed to hold the essential components which can be easily adjusted to meet the different requirements.

The software system is comprised of several functional modules as illustrated in Fig. 3. The tracking module deals with the tracking of physical objects, including the microsurgical instruments and artificial blood vessels. The motion and deformation data are collected and utilized to drive the simulation process. The rendering module generates realistic rendering frames which are then presented to the final display module and observed by users.

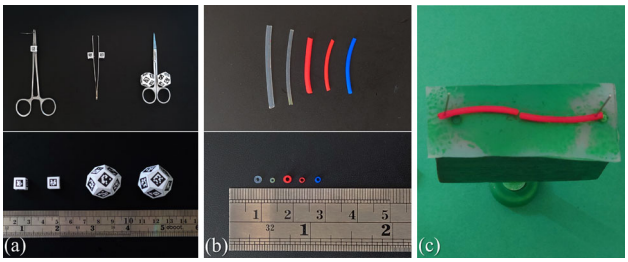


**Fig. 4** Microsurgical instruments and soft silicone tubes. **a** Microsurgical instruments with fiducial platonic solids. The marker lengths of the hexahedron and dodecahedron solids are $5.1mm$ and $7.5mm$, respectively. **b** Silicone tubes with different sizes are employed as the artificial blood vessels. **c** Operating area. The tubes with $0.7mm$ wall thickness and $2.0mm$ diameter are used for the simulation

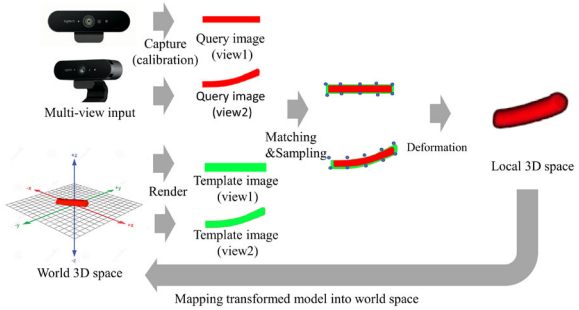


**Fig. 5** Workflow of the shape matching-based tracking and mapping approach

## 4 Vision-based tracking system

### 4.1 Tacking of microsurgical instruments

The tracking of a single rigid object refers to estimating the six-degrees-of-freedom (6DoF) pose of the target object. The pose $\mathbf{T}$ can be represented as a rotation $\mathbf{R} \in \mathbb{SO}(3)$ and a translation $\mathbf{t} \in \mathbb{R}^3$ so that the target pose can be described as:$\mathbf{T} = \begin{bmatrix} \mathbf{R} & \mathbf{t} \\ \mathbf{0} & 1 \end{bmatrix} \in \mathbb{SE}(3)$, where $\mathbb{SO}(3)$ is the special orthogonal group, and pose $\mathbf{T}$ is an element of the special Euclidean group $\mathbb{SE}(3)$. The pose is a transformation process between the local coordinate space and the camera's. Let $\hat{\mathbf{x}}_i = [x_i, y_i, z_i]^T \in \mathbb{R}^3$ be the 3D points in the local space and $\mathbf{x}_i = [u_i, v_i]^T \in \mathbb{R}^2$ be the corresponding 2D points in the image plane. Then, the relationship between these two sets of points is given by:

$$\mathbf{x}_i = \pi(\mathbf{K}\mathbf{T}\hat{\mathbf{x}}_i) = \pi(\mathbf{K}[\mathbf{R}|\mathbf{t}]\,[x_i, y_i, z_i, 1]^T),$$

where $\pi(\hat{\mathbf{x}}) = [x/z, y/z]^T$ is the projection operator and $\mathbf{K} \in \mathbb{R}^{3\times3}$ is the camera intrinsic matrix that can be obtained from an offline calibration step.

However, the microsurgical instruments with local mechanical motions, such as the shearing motion of scissors and the clamping motion of forceps, cannot be modeled as the simple 6DoF pose. In this work, we treat the compound motion as a combination of several local motions and integrate the TsFPS [15] into our tracking system. As shown in Fig. 4a, the fiducial platonic solids (FPSs) are attached onto the instruments. The trajectories can be recovered by continuously estimating the pose of each FPS. Experimental results of the instrument tracking are demonstrated in Sect. 7.

### 4.2 Non-rigid object tracking and simulation

We propose a semi-dense method for the soft tissue tracking instead of the dense tracking. For a single frame in the loop, a fast shape matching method is utilized to extract the edge points of the soft tissues from multi-view images. These points are then mapped to the 3D models for the deformation simulation via the PBD method [48]. Figure 5 shows the overview of the workflow. Algorithm 1, meanwhile, demonstrates the detail of our method.

**Algorithm 1** Soft Tissue Tracking

1: **for all** views **do**
2: $\quad\mathbf{P}_k$ : ShapeMatching($\mathbf{U}_k, \mathbf{V}_k$)
3: **end for**
4: $\hat{\mathbf{P}}$ : ValidPointPairsFilter($\{\mathbf{P}_k\}$)
5: $\mathbf{x}$ : Triangulation($\mathbf{T}, \hat{\mathbf{P}}$)
6: $\mathbf{X}$ : UpdateFeatureVertices($\mathbf{x}$)
7: **while** $count < solveIterations$ **do**
8: $\quad$PBDConstraintSolver($\mathbf{X}$)
9: $\quad count = count + 1$
10: **end while**
11: UpdatePositions($\mathbf{X}$)
12: UpdateVelocities($\mathbf{X}$)

Let $\mathbf{U}_k = \{u_i\}$ and $\mathbf{V}_k = \{v_j\}$ be the sets of edge maps for the template images (rendered from underlying 3D models) and the query images (captured from cameras), respectively. $k$ is the camera id, and $u_i$ and $v_j$ are the points of the edges. The camera system $\mathbf{C} = \{C_k\}$ captures streaming data from different views, where $\mathbf{T} = \{T_k\}$ is the pose of the camera. $\mathbf{P}_k$ is the sampled feature pairs based on the matched shapes. The vertices of the underlying model are denoted as $\mathbf{x} \in \mathbb{R}^{n\times3}$. Lines (1)–(3) show that the shape matching is the first step in each loop. The typical chamfer distance between $\mathbf{U}$ and $\mathbf{V}$ is $D_{cm} = \frac{1}{n}\sum_{u_i\in\mathbf{U}} \min_{v_j\in\mathbf{V}} |u_i - v_j|$. The value is given by mean distance between each point in $U$ and its nearest edge in $V$. To achieve a more robust matching, we employ the directional chamfer distance [49, 50] which adds a directional term to the left. The directional chamfer distance is given by:

$$D_{dcm}(\mathbf{U}, \mathbf{V}) = \frac{1}{n}\sum_{u_i\in\mathbf{U}} \min_{v_j\in\mathbf{V}} |u_i - v_j| + \lambda|\phi(u_i) - \phi(v_j)|.$$

where the first term is a standard chamfer matching distance and the second is a penalty term for directions. $\lambda$ is a weighting factor between the chamfer score and the directional score. The direction $\phi(x)$ is represented as the angle between the horizontal line and the tangential direction.

After the shape matching process, a set of point pairs $\mathbf{P}_k = \{[u_i, v_j]\}$ is obtained by uniformly sampling the template and query edge maps. The points of template maps have the corresponding 3D vertices $\mathbf{x}$ which can be inferred from the Frame Buffer. Thus, the valid point pairs $\hat{\mathbf{P}}$ are acquired by applying a simple logical AND operation to all sets of point pairs $\{\mathbf{P}_1, ..., \mathbf{P}_k\}$ as shown in Line (4) of the Algorithm 1. By giving the valid point pairs $\hat{\mathbf{P}}$ and camera poses $T$, the 3D positions of the vertices $\mathbf{x}$ can be obtained by triangulation [51]. Lines (7)–(10) represent the procedure of PBD that provides an efficient and visually plausible simulation for deformable objects. The number of iterations is a constant which directly affects the computation efficiency and accuracy of the results. A larger number leads to visually more plausible but increases the computational burden.

## 5 Anatomical modeling

### 5.1 Method overview

As mentioned, we use an end-to-end learning-based framework for anatomical modeling, which is presented in more detail in this section. This framework is inspired by (1) patient-specific modeling approach that reconstructs anatomical models from the patient-specific data [16] and (2) recent deep learning work in recovering 3D shapes from single 2D images [52, 53]. Figure 6 shows the overview of the framework, including data acquisition, network training, and testing procedures. The design follows a two-step strategy [53]. A CGANs architecture is used to train a generator that converts X-ray images to normal images. These normal images provide the silhouette and geometric constraints to the CNNs for the mesh predictor training. The architecture of the encoder–decoder CNNs is identical to that of the prior work [53]. A differentiable renderer is incorporated into the framework; it provides approximate gradients for the rendering process, which leads to the successful integration of the 3D rendering pipeline into neural networks. By introducing this differentiable renderer, the bridge of error propagation between 2D image data 3D spatial data is built, thus enabling easier training for the mesh predictor without any 3D supervision.

The output model is deformed from a predefined template mesh. The deformation process is formulated as $v_i + \triangle v_i^l + \triangle v^g$, where $v_i$ is the vertex of the mesh, $\triangle v_i^l$ is the local bias for each vertex, and $\triangle v^g$ is a global bias. These two bias vectors are the outputs of the mesh predictor. For each category of the anatomy structure, a neutral predefined anatomical mesh is used as the underlying template model. The objective is a simple function based on the 2D image distance benefits from the incorporation of the differentiable renderer. The objective function consists of an intersection-over-union (IOU) term, a normal loss that is the $L1$ norm distance between the normal images, and a smoothness loss [53, 55] which is utilized to keep the consistency of the mesh surface.

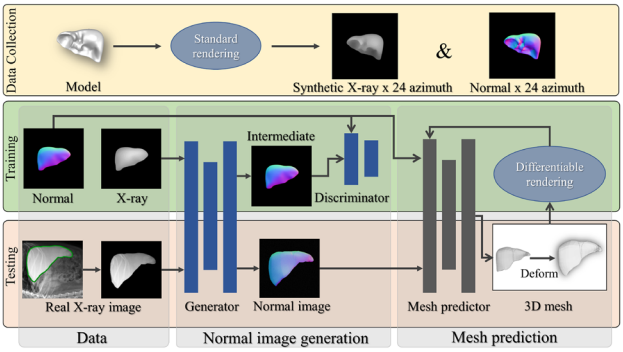


**Fig. 6** The overview of the modeling framework. The framework consists of a CGANs [54] architecture for normal image generation and an encoder–decoder CNNs architecture for mesh prediction. The training data include synthetic X-ray images and normal images, both of which are obtained by rendering from a anatomical model dataset

### 5.2 Data acquisition

This 3D modeling module aims to recover the anatomical model from a single 2D X-ray image. Massive amounts of 2D medical imaging data and 3D models are required for training the networks. However, there is no such a large-scale medical image dataset which contains corresponding anatomical mesh models. Thus, an artificial medical image generation pipeline is introduced in this work. It is built upon a standard rendering pipeline with a normal shader and an X-ray shader. The normal generation is a conversion between the surface normals and RGB values. The X-ray shader is developed upon the relative depth of the mesh. By reading data from the Z-buffer, the relative depth value can be given by: $D = 1 - \frac{z - d_{\min}}{d_{\max} - d_{\min}}$, where $z$ is the depth value of the vertex and $d_{\max}$ and $d_{\min}$ represent the furthest and nearest distances of the vertices with respect to the current angle of view. It in line with the imaging principle of the X-ray scan that is the penetration depths of X-ray photon [56]. By introducing these two shaders, our rendering pipeline can efficiently generate both synthetic X-ray images and normal images. We generate and collect a spine dataset and a liver dataset for our experiments (see Sect. 7). The spine is a skeleton structure and the liver is a soft tissue, which are two representative human anatomical structures. Furthermore, the liver mesh is used in a prototype development that is presented in Sect. 6.

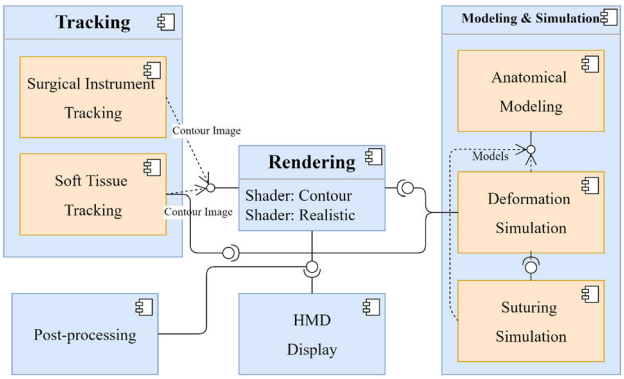


**Fig. 7** Component diagram of the system

## 6 Prototype development

In this section, we present a prototype system based on our framework. Besides the tracking and modeling modules, rendering and suturing modules are introduced to create an interactive simulation for the microsurgery in **microvascular hepatic artery reconstruction** (MHAR). From the perspective of software engineering, all the functional modules are organized into five subsystems as shown in Fig. 7. This prototype system is developed by using C++ and OpenGL API, please refer to Sect. 7 for more details of the development platform.

**Tracking.** The proposed tracking system is implemented. Hexahedron FPSs with 5.1 mm marker length and dodecahedron FPSs with 7.5 mm marker length are used for tracking needle, holder, forceps and scissors (see Fig. 4). Soft tubes with 0.7 mm wall thickness and 2.0 mm diameter are employed as the artificial blood vessels, which are the typical synthetic models in traditional training simulators [20].

**Modeling and Rendering.** A 3D liver model is used to create a virtual environment for the simulation. This mesh model is generated via our learning-based anatomical modeling method. We employed a neutral liver shape mesh with 642 vertices as the predefined template in the training and testing processes. In addition, to create an immersive virtual environment, a physics-based rendering (PBR) [57] pipeline with specialized materials is introduced to provide efficient and realistic rendering to our prototype system. The surface parameters for PBR can be given by different textures. A couple of texture layers provide base color, scattering, normal, extra shadow and roughness parameters to our rendering pipeline. The result is demonstrated in Sect. 7.

**Suturing Simulation.** A few studies have been undertaken on surgical suturing simulation. Xu and Liu [58] use the PBD model to simulate the inextensible surgical thread. Yu et al. [59] propose a two-stage interaction strategy for the virtual suturing simulation in a VR-based laparoscopic surgery simulator. However, these methods cannot be applied directly to a mixed reality scenario. Based on a region tracking method and the PBD deformation model, we introduce a tracking-aware approach for the suturing simulation.

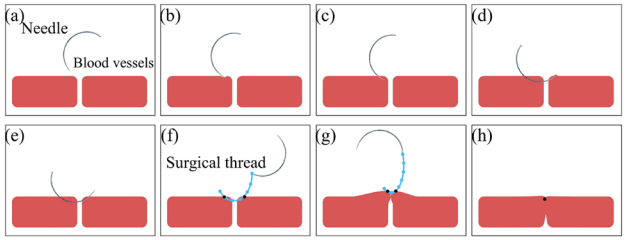


**Fig. 8** Suturing simulation. **a Idle**: there is no contact between the needle and the blood vessel. **b Puncture (in) resistance**: first contact between the head of the needle and the blood vessel with small deformation. **c Puncturing**: the needle pierces into the blood vessel. **d Puncture (out) resistance**: the needle is trying to penetrate out the vascular wall with small local deformation. **e Puncture out**: the needle punctures through both blood vessels. **f Threading**: the surgical thread is passing through the blood vessels. **g Closing**: when the last thread knot (blue) hits on the outer wall of the blood vessel, the blood vessels deform to close to each other by moving the vertices of the insertion knots (black). **h Idle**: one suturing loop is completed

This procedure is divided into six phases: Idle, Puncture resistance, Puncturing, Puncture out, Threading, and Closing; more details are shown in Fig. 8. Steps a–f demonstrate the interaction between the needle and the blood vessels. g–i show the stitching process. The position of the needle head can be recovered by estimating the underlying needle model via region-based constraints. The trigger of each step is based on the tracking results of the needle and soft tubes along with collision detection.

## 7 Experiments

In this section, we present the experimental results and evaluations, a user study is conducted as well to demonstrate the validity of the framework. Please note that all of these experiments are conducted under a Windows 10 PC equipped with a 8 Cores 3.6 GHz CPU (*Intel Core i9-9900KF*), 32 GB of RAM, a GPU (*Nvidia RTX 2080Ti*) with 11GB of GDDR6 memory capacity, and an *Oculus Rift* HMD. Two *Logitech* webcams (1280 × 720, 60fps) and a *ZED mini* stereo camera (2560 × 720, 60fps) are employed to construct the camera system.

### 7.1 Tracking result

Our proposed vision-based system provides accurate and robust tracking for multiple microsurgical instruments and soft tubes. As shown in Fig. 4, in the microsurgery simulation scenario, the tracking targets are a needle, holder, forceps,

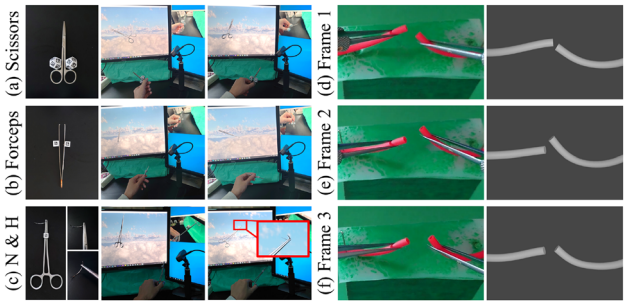


**Fig. 9** **a** Tracking of microsurgical instruments. **b** Three randomly selected frames that show the tracking and simulation results of two blood vessels

**Table 1** Tracking accuracy and stability evaluation. $E_t$ and $E_r$ represent the translation error ($mm$) and rotation error (°), respectively. $S_r$ and $S_t$ are the standard deviation of $E_t$ and $E_r$

| Marker type | $E_t$ | $E_r$ | $S_t$ | $S_r$ |
|---|---|---|---|---|
| Scissors | 0.71 | 0.15 | 0.30 | 0.13 |
| Forceps | 2.98 | 1.43 | 1.85 | 0.57 |
| Needle holder | 1.12 | 0.65 | 0.79 | 0.38 |

scissors, and soft silicone tubes. The experiment is conducted in an indoor environment with natural illumination. Figure 9 shows some results.

The accuracy and stability of the rigid tracking are evaluated by synthetic testing data, which are suggested in prior work [15, 60]. The synthetic data are a series of sequential frames of one or two (depending on the instrument type) platonic solids' motion trajectories, which are rendered via a standard rendering pipeline. The Rotation and Translation data are recorded as the ground truth $\{\hat{\mathbf{R}}|\hat{\mathbf{t}}\}$, while the tracking result $\{\mathbf{R}|\mathbf{t}\}$ is estimated by applying our tracking method to the synthetic data. Then, the rotation error and the translation error of each solid are given by $E_r = \arccos\left((Tr(\mathbf{R}^T\hat{\mathbf{R}}) - 1)/2\right)$ and $E_t = ||\mathbf{t} - \hat{\mathbf{t}}||$. In addition to the accuracy evaluation, the standard deviation of errors is calculated to evaluate the tracking stability for each instrument. Results are presented in Table 1; it shows that our approach can achieve millimeter and even submillimeter accuracy.

## 7.2 Modeling result

There are 36 liver models (31 for training, 5 for testing) and 66 spine vertebra models (57 for training, 9 for testing) are collected to generate datasets. For each 3D model, both synthetic X-ray images and normal images are rendered under 24 azimuth angles. The resolution of the images is $256 \times 256$. Figure 10a shows some samples data. After completing the training processes, a normal image generator and a mesh predictor are obtained. In the testing process, the input X-ray image is extracted from a real X-ray scan and is then transferred to the generator for normal image generation. Subsequently, the mesh predictor takes the generated normal image as input for mesh reconstruction. Some experimental results can be found in Fig. 10. Please note that, because our work focuses on 3D model reconstruction, the experiment is built upon a segmentation assumption as shown in Fig. 10b, the valid area is highlighted by the green contour line based on a segmentation assumption. As mentioned earlier, the PBR pipeline can get object surface parameters from different textures. Thus, we use a couple of texture layers to provide base color, scattering, normal, extra shadow and roughness parameters. This procedure and the rendering result are illustrated in Fig. 11.

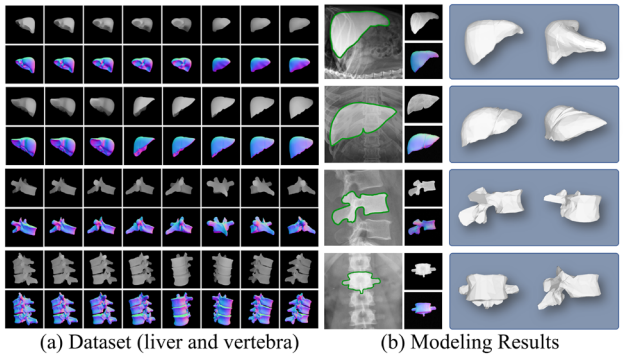


**Fig. 10** **a** Samples of training data. **b** Results of the liver and single vertebra reconstruction

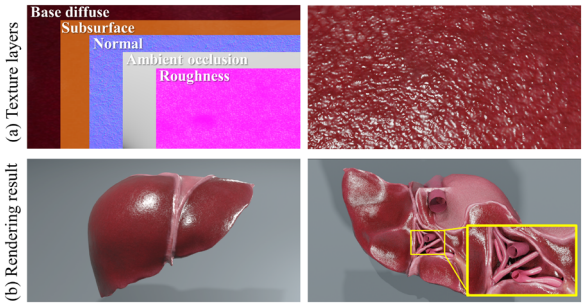


**Fig. 11** Realistic rendering. **a** Texture layers and surface details of the liver model. **b** Render results of a liver model. Blood vessel meshes are built and assembled with the liver, as shown in the highlight area

## 7.3 MHAR simulator

The experiment is conducted under a stable light condition as shown in Fig. 12. Users are able to feel the real tactile force by using real microsurgical instruments. The motion and deformation data are captured for simulation. The realistic rendering frames are finally presented to users via the goggles. To evaluate the performance efficiency, a real-time analysis program is applied. There are four stages denoted in Fig. 13. Its performance is acquired by calculating the frame

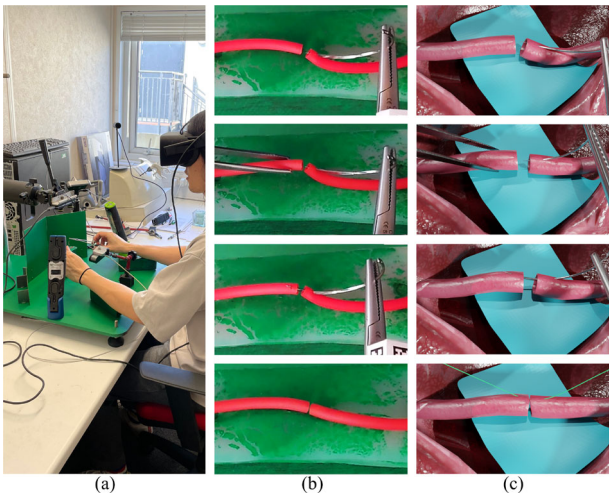


**Fig. 12** A prototype of MR-based MHAR simulation. **a** User is allowed to use real microsurgical instruments instead of haptic devices. **b** Input frames that are captured by a camera. **c** Output frames that are presented to the user via the HMD

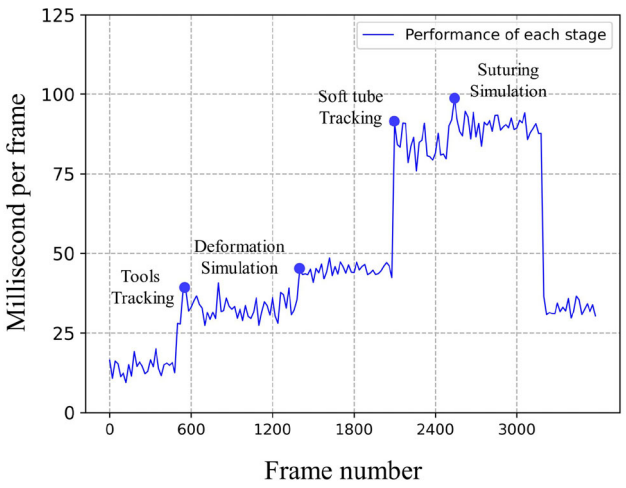


**Fig. 13** Real-time performance analysis

rate within a sequence of frames. The experimental data are sampled from 3621 frames. The average rendering rate is 20.25 frames per second with the resolution of 1280 pixels by 720 pixels for each eye.

In addition, a post-processing module is developed and incorporated into the system. It is an optional functional module, which allows programs to edit the final output frames, such as adding image effects, adjusting image properties. Figure 14 shows a matting and compositing process.

To further evaluate the validation of this prototype system and the framework, we conducted a small-scale user study with 5 participants (aged 27–68), one of them is a senior microsurgeon, others are average people. They were asked to do some basic operations such as observing the virtual scene, operating real instruments, and suturing. During the

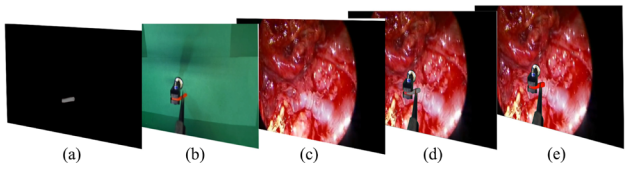


**Fig. 14** A frame breakdown of compositing output. **a** 3D vascular model. **b** Input frame captured by the top-view camera. **c** Background image, it also can be a surgery video or a real-time rendering virtual scene of human internal organs. **d** and **e** Compositing outputs. Soft tube is replaced with the real-time rendering vascular model; the green background is changed to a real microsurgery picture

experiment, participants were asked to grade our framework via Chan's validation method for the microsurgery simulator [4, 7], which is based on users' subjective experiences. The evaluation metrics is comprised of five aspects: *Face Validity* refers to the degree to which the simulator resembles the real surgical scenarios. *Content Validity* measures the ability to assess a specific microsurgical skill, not other general knowledge. *Construct Validity* represents whether the simulator can differentiate skill levels among the users including beginners and experts. *Concurrent Validity* indicates whether the simulator is comparable to the existing gold standard or ground truth. *Predictive Validity* measures how much the simulation training improved actual surgical skills.

The score given by participants is based on the comparison among prior microsurgery simulators that are validated by Chan et al. [4]. The scores for prior simulators are retained and used as the reference. We collect feedback from all five participants and calculate the average rating for each validity. Table 2 shows the result that demonstrates our framework makes a considerable improvement in microsurgery simulation especially in the realism (*Face Validity*), and achieves good results in *Content Validity* primarily because it was specifically developed for microanastomosis techniques. The positive rating in *Concurrent Validity* reveals that the MR-based simulation has the potential to become an effective supplement to the traditional "gold standard" training model. The success in achieving these promising results can be attributed to two main factors. Firstly, the introduction of modern rendering techniques has significantly improved the graphics of our system compared to systems developed over a decade ago. Secondly, the proposed visual-tactile mechanism provides a stronger sense of immersion for users, making the experience more realistic and closer to an actual surgical scenario.

## 8 Conclusion

We present an MR framework for the MR-based microsurgery simulation, which provides users with real tactile feedback instead of the simulated force from HFDs. A vision-

**Table 2** Validation and Comparison

| Simulators | Face validity | Content validity | Construct validity | Concurrent validity | Predictive validity |
|---|---|---|---|---|---|
| Senior's Microvascular simulator [61] | + | ++ | ++ | – | – |
| Boston Dynamics Inc. Surg simulator [29] | ++ | ++ | +++ | – | – |
| Algorithmic tools [62] | +++ | +++ | ++ | – | – |
| Hand-motion analysis [63] | + | +++ | +++ | – | – |
| MHAR simulator (ours) | +++++ | ++++ | +++ | ++ | – |

based tracking system is proposed to capture the motion and deformation data for the simulation, which is one of the core components of our framework. A learning-based modeling method is proposed to generate the anatomical 3D models for the simulation of different microsurgical specialities. Other components including suturing simulation, deformation simulation, realistic rendering, and post-processing are also introduced. A prototype system is developed based on this framework. Experimental results and user study have shown both the feasibility and potentiality of our framework. This work represents a solid first step in the development of virtual surgery using MR technologies.

**Limitations.** Although this work achieves some promising results, there are still some difficult challenges that need to be studied and solved. The real-time performance of the system is critical to the user experience; however, simultaneously tracking multiple surgical tools and soft tubes dramatically increases the computational burden and affects the final performance of our current system (see Fig. 13). The unstable frame rate directly affects the system evaluation and user experience. The long-standing problems of vision-based tracking have been alleviated but not yet solved. Tracking performance may still suffer when there is illumination variation, motion blur, and partial occlusion. In addition, the prototype system is developed mainly to demonstrate the feasibility of the framework pipeline. Current user study is too small and simple, which is far from comprehensive; therefore, the user study and the usability evaluation need to be further strengthened and improved.

**Future work.** The main functional modules of the framework are implemented on CPU except the rendering process. Some GPU-based virtual surgery systems have demonstrated that the GPU accelerated computing can tremendously improve the real-time performance of the system. Therefore, a GPU-based implementation is imperative for the follow-up development of our framework. Increasing the number of sensors and introducing high-speed cameras to the framework can be an effective approach to improve the robustness of the tracking system. The balance between computing resource and sensor quantity should be studied properly. Learning-based methods on image illumination and de-noising are also worth exploring. Furthermore, a more comprehensive evaluation scheme would be conducted in the near future.

**Acknowledgements** This work was supported by XJTLU Research Development Fund No. RDF-21-02-065 and Neuravatar Project funded by High Education Innovation Fund (UK-HEIF).

## References

1. Tamai, S.: History of microsurgery. Plast. Reconstr. Surg. **124**(6S), e282–e294 (2009)
2. Microsurgeon.org: Microsurgery definition. https://www.microsurgeon.org/microsurgerydef, (2021) Accessed on 08 Apr 2021
3. Roohi, S.A.: Tips and tricks in microvascular anastomoses. In: The Current Perspectives on Coronary Artery Bypass Grafting. IntechOpen (2020)
4. Chan, W.Y., Matteucci, P., Southern, S.J.: Validation of microsurgical models in microsurgery training and competence: a review. Microsurg. Off. J. Int. Microsurg. Soc. Eur. Fed. Soc. Microsurg. **27**(5), 494–499 (2007)
5. Byvaltsev, V.A., Akshulakov, S.K., Polkin, R.A., Ochkal, S.V., Stepanov, I.A., Makhambetov, Y.T., Kerimbayev, T.T., Staren, M., Belykh, E., Preul, M.C.: Microvascular anastomosis training in neurosurgery: A review. Minim. Invasive Surg. (2018). https://doi.org/10.1155/2018/6130286
6. Javid, P., Aydın, A., Mohanna, P.N., Dasgupta, P., Ahmed, K.: Current status of simulation and training models in microsurgery: a systematic review. Microsurgery **39**(7), 655–668 (2019)
7. Crouch, G., Wong, G., Hong, J., Varey, A., Haddad, R., Wang, Z.Z., Wykes, J., Koutalistras, N., Clark, J.R., Solomon, M., et al.: Validated specialty-specific models for multi-disciplinary microsurgery training laboratories: a systematic review. ANZ J. Surg. **91**(6), 1110–1116 (2021)
8. Hosain, M.: Microsurgery training: are the live models era coming in to the tail?–a literature review. Journal of Advances in Medicine and Medical Research pp. 97–109 (2021)
9. StandfordMedicine: Microsurgery essentials. https://plasticsurgery.stanford.edu/education/microsurgery.html, (2021) Accessed 20 Aug 2021
10. Wanderer, S., Waltenspuel, C., Grüter, B.E., Strange, F., Sivanrupan, S., Remonda, L., Widmer, H.R., Casoni, D., Andereggen, L., Fandino, J., et al.: Arterial pouch microsurgical bifurcation aneurysm model in the rabbit. JoVE J. Vis. Exp. **159**, e61157 (2020)
11. Erel, E., Aiyenibe, B., Butler, P.E.: Microsurgery simulators in virtual reality. Microsurg. Offi. J. Int. Microsurg. Soc. Eur. Fed. Soc. Microsurg. **23**(2), 147–152 (2003)
12. Hoshyarmanesh, H., Zareinia, K., Lama, S., Sutherland, G.R.: Structural design of a microsurgery-specific haptic device: neuroarmplushd prototype. Mechatronics **73**, 102481 (2021)

13. Rangarajan, K., Davis, H., Pucher, P.H.: Systematic review of virtual haptics in surgical simulation: A valid educational tool? J. Surg. Educ. **77**(2), 337–347 (2020)
14. Yang, L., Etsuko, K.: Review on vision-based tracking in surgical navigation. IET Cyber-Syst. Robot. **2**(3), 107–121 (2020)
15. Xiang, N., Yang, X., Zhang, J.J.: Tsfps: An accurate and flexible 6dof tracking system with fiducial platonic solids. In: Proceedings of the 29th ACM International Conference on Multimedia, pp. 4454–4462 (2021)
16. Neal, M.L., Kerckhoffs, R.: Current progress in patient-specific modeling. Brief. Bioinform. **11**(1), 111–126 (2010)
17. Bücking, T.M., Hill, E.R., Robertson, J.L., Maneas, E., Plumb, A.A., Nikitichev, D.I.: From medical imaging data to 3d printed anatomical models. PloS one **12**(5), e0178540 (2017)
18. Birbara, N.S., Otton, J.M., Pather, N.: 3d modelling and printing technology to produce patient-specific 3d models. Heart Lung Circ. **28**(2), 302–313 (2019)
19. Fanua, S.P., Kim, J., Shaw Wilgis, E.: Alternative model for teaching microsurgery. Microsurgery **21**(8), 379–382 (2001)
20. Atlan, M., Lellouch, A.G., Legagneux, J., Chaouat, M., Masquelet, A.C., Letourneur, D.: A new synthetic model for microvascular anastomosis training? A randomized comparative study between silicone and polyvinyl alcohol gelatin tubes. J. Surg. Educ. **75**(1), 182–187 (2018)
21. Xiao, Z., Samii, M., Wang, J., Pan, Q., Xu, Z., Ju, H.: Training model for the intraluminal continuous suturing technique for microvascular anastomosis. Sci. Rep. **11**(1), 1–9 (2021)
22. Remie, R.: The pvc-rat and other alternatives in microsurgical training. Lab. Anim. **30**(9), 48–52 (2001)
23. De Virgilio, A., Costantino, A., Ebm, C., Conti, V., Mondello, T., Di Bari, M., Cugini, G., Mercante, G., Spriano, G.: High definition three-dimensional exoscope (vitom 3d) for microsurgery training: a preliminary experience. Eur. Arch. Otorhinolaryngol. **277**(9), 2589–2595 (2020)
24. Chen, W.F., Eid, A., Yamamoto, T., Keith, J., Nimmons, G.L., Lawrence, W.T.: A novel supermicrosurgery training model: the chicken thigh. J. Plast. Reconst. Aesthet. Surg. **67**(7), 973–978 (2014)
25. Creighton, F.X., Feng, A.L., Goyal, N., Emerick, K., Deschler, D.: Chicken thigh microvascular training model improves resident surgical skills. Laryngoscope Investig. Otolaryngol. **2**(6), 471–474 (2017)
26. de Giacomo Carneiro, C., Scapini, F.: The rabbit as an experimental model in laryngology (2009)
27. Yamamoto, T., Yamamoto, N., Yamashita, M., Furuya, M., Hayashi, A., Koshima, I.: Establishment of supermicrosurgical lymphaticovenular anastomosis model in rat. Microsurgery **37**(1), 57–60 (2017)
28. Rodríguez, A., Álvarez, Á., Aguirrezabalaga, J., Martelo, F.: The anteromedial thigh flap as a training model of a perforator flap in rat. J. Reconstr. Microsurg. **23**(05), 251–255 (2007)
29. Otoole, R.V., Playter, R.R., Krummel, T.M., Blank, W.C., Cornelius, N.H., Roberts, W.R., Bell, W.J., Raibert, M.: Measuring and developing suturing technique with a virtual reality surgical simulator. J. Am. Coll. Surg. **189**(1), 114–127 (1999)
30. Kazemi, H., Rappel, J.K., Poston, T., Hai Lim, B., Burdet, E., Leong Teo, C.: Assessing suturing techniques using a virtual reality surgical simulator. Microsurgery **30**(6), 479–486 (2010)
31. Alaraj, A., Luciano, C.J., Bailey, D.P., Elsenousi, A., Roitberg, B.Z., Bernardo, A., Banerjee, P.P., Charbel, F.T.: Virtual reality cerebral aneurysm clipping simulation with real-time haptic feedback. Oper. Neurosurg. **11**(1), 52–58 (2015)
32. Ryu, J., Choi, J., Kim, H.C.: Endoscopic vision-based tracking of multiple surgical instruments during robot-assisted surgery. Artif. Organs **37**(1), 107–112 (2013)
33. Yang, L., Wang, J., Ando, T., Kubota, A., Yamashita, H., Sakuma, I., Chiba, T., Kobayashi, E.: Vision-based endoscope tracking for 3d ultrasound image-guided surgical navigation. Comput. Med. Imaging Graph. **40**, 205–216 (2015)
34. Sánchez-González, P., Cano, A.M., Oropesa, I., Sánchez-Margallo, F.M., Pozo, F.D., Lamata, P., Gómez, E.J.: Laparoscopic video analysis for training and image-guided surgery. Minim. Invasive Ther. Allied Technol. **20**(6), 311–320 (2011)
35. Robu, M., Kadkhodamohammadi, A., Luengo, I., Stoyanov, D.: Towards real-time multiple surgical tool tracking. Comput. Methods Biomech. Biomed. Eng. Imaging Vis. pp. 1–7 (2020)
36. Liu, X., Plishker, W., Shekhar, R.: Hybrid electromagnetic-aruco tracking of laparoscopic ultrasound transducer in laparoscopic video. J. Med. Imaging **8**(1), 015001 (2021)
37. Gadwe, A., Ren, H.: Real-time 6dof pose estimation of endoscopic instruments using printable markers. IEEE Sens. J. **19**(6), 2338–2346 (2018)
38. Richa, R., Poignet, P., Liu, C.: Three-dimensional motion tracking for beating heart surgery using a thin-plate spline deformable model. Int. J. Robot. Res. **29**(2–3), 218–230 (2010)
39. Wong, W.K., Yang, B., Liu, C., Poignet, P.: A quasi-spherical triangle-based approach for efficient 3-d soft-tissue motion tracking. IEEE/ASME Trans. Mechatron. **18**(5), 1472–1484 (2012)
40. Yang, B., Wong, W.K., Liu, C., Poignet, P.: 3d soft-tissue tracking using spatial-color joint probability distribution and thin-plate spline model. Pattern Recogn. **47**(9), 2962–2973 (2014)
41. Schoob, A., Kundrat, D., Kahrs, L.A., Ortmaier, T.: Stereo vision-based tracking of soft tissue motion with application to online ablation control in laser microsurgery. Med. Image Anal. **40**, 80–95 (2017)
42. Song, J., Wang, J., Zhao, L., Huang, S., Dissanayake, G.: Dynamic reconstruction of deformable soft-tissue with stereo scope in minimal invasive surgery. IEEE Robot. Autom. Lett. **3**(1), 155–162 (2017)
43. Antiga, L., Piccinelli, M., Botti, L., Ene-Iordache, B., Remuzzi, A., Steinman, D.A.: An image-based modeling framework for patient-specific computational hemodynamics. Med. Biol. Eng. Comput. **46**(11), 1097–1112 (2008)
44. Taylor, C.A., Figueroa, C.: Patient-specific modeling of cardiovascular mechanics. Annu. Rev. Biomed. Eng. **11**, 109–134 (2009)
45. Tahir, W., Kura, S., Zhu, J., Cheng, X., Damseh, R., Tadesse, F., Seibel, A., Lee, B.S., Lesage, F., Sakadžic, S., et al.: Anatomical modeling of brain vasculature in two-photon microscopy by generalizable deep learning. BME Frontiers **2021** (2021)
46. Bhalodia, R., Elhabian, S.Y., Kavan, L., Whitaker, R.T.: Deepssm: A deep learning framework for statistical shape modeling from raw images. In: International Workshop on Shape in Medical Imaging, pp. 244–257. Springer (2018)
47. Kong, F., Wilson, N., Shadden, S.C.: A deep-learning approach for direct whole-heart mesh reconstruction. arXiv preprint arXiv:2102.07899 (2021)
48. Müller, M., Heidelberger, B., Hennix, M., Ratcliff, J.: Position based dynamics. J. Vis. Commun. Image Represent. **18**(2), 109–118 (2007)
49. Liu, M.Y., Tuzel, O., Veeraraghavan, A., Chellappa, R.: Fast directional chamfer matching. In: 2010 IEEE Computer Society Conference on Computer Vision and Pattern Recognition, pp. 1696–1703. IEEE (2010)
50. Yu, Q., Wei, H., Yang, C.: Local part chamfer matching for shape-based object detection. Pattern Recogn. **65**, 82–96 (2017)
51. Hartley, R.I., Sturm, P.: Triangulation. Computer vision and image understanding **68**(2), 146–157 (1997)
52. Liu, S., Li, T., Chen, W., Li, H.: Soft rasterizer: A differentiable renderer for image-based 3d reasoning. In: Proceedings of the IEEE International Conference on Computer Vision, pp. 7708–7717 (2019)

53. Xiang, N., Wang, R., Jiang, T., Wang, L., Li, Y., Yang, X., Zhang, J.: Sketch-based modeling with a differentiable renderer. Comput. Anim. Virtual Worlds **31**(4–5), e1939 (2020)
54. Mirza, M., Osindero, S.: Conditional generative adversarial nets. arXiv preprint arXiv:1411.1784 (2014)
55. Kato, H., Ushiku, Y., Harada, T.: Neural 3d mesh renderer. In: Proceedings of the IEEE Conference on Computer Vision and Pattern Recognition, pp. 3907–3916 (2018)
56. WirelessWorld: Advantages of x-ray | disadvantages of x-ray. https://www.rfwireless-world.com/Terminology/Advantages-and-Disadvantages-of-X-Ray.html (2021), Accessed on 15 Aug 2021
57. Pharr, M., Jakob, W., Humphreys, G.: Physically based rendering: from theory to implementation. Morgan Kaufmann (2016)
58. Xu, L., Liu, Q.: Real-time inextensible surgical thread simulation. Int. J. Comput. Assist. Radiol. Surg. **13**(7), 1019–1035 (2018)
59. Yu, P., Pan, J., Qin, H., Hao, A., Wang, H.: Real-time suturing simulation for virtual reality medical training. Comput. Anim. Virtual Worlds **31**(4–5), e1940 (2020)
60. Wu, P.C., Wang, R., Kin, K., Twigg, C., Han, S., Yang, M.H., Chien, S.Y.: Dodecapen: Accurate 6dof tracking of a passive stylus. In: Proceedings of the 30th Annual ACM Symposium on User Interface Software and Technology, pp. 365–374 (2017)
61. Senior, M.A., Southern, S.J., Majumder, S.: Microvascular simulator-a device for micro-anastomosis training. Ann. R. Coll. Surg. Engl. **83**(5), 358 (2001)
62. Brown, J., Sorkin, S., Latombe, J.C., Montgomery, K., Stephanides, M.: Algorithmic tools for real-time microsurgery simulation. Med. Image Anal. **6**(3), 289–300 (2002)
63. Grober, E.D., Hamstra, S.J., Wanzel, K.R., Reznick, R.K., Matsumoto, E.D., Sidhu, R.S., Jarvi, K.A.: Validation of novel and objective measures of microsurgical skill: hand-motion analysis and stereoscopic visual acuity. Microsurgery **23**(4), 317–322 (2003)




**Nan Xiang** is a Lecturer at the Department of Computing, Xi'an Jiaotong-Liverpool University. He received his BS degree (2012) in software engineering from Nanchang University (China), MA (2017), in animation from Communication University of China, and PhD (2021) in computer animation from National Centre for Computer Animation, Bournemouth University (UK). His current research interests include 3D reconstruction, computer animation, virtual surgery, and XR technologies.

**Lingyun Yu** is an Associate Professor at the Department of Computing, Xi'an Jiaotong-Liverpool University. She obtained the PhD degree on Scientific Visualization and Interaction Techniques from the University of Groningen in 2013. After that, she worked as a Lecturer and Associate Researcher at Hangzhou Dianzi University from 2014 to 2017, and a Postdoctoral Research Fellow at the University of Groningen and the University Medical Center Groningen from 2016 to 2019. Her research focuses on interactive visualization, immersive visualization, human-computer interaction and virtual/augmented reality.

**Hai-Ning Liang** is Professor of Computing and inaugural Head of the Department of Computing at Xi'an Jiaotong-Liverpool University (XJTLU), Suzhou, China. He is also Deputy Director of the Suzhou Key Laboratory of Intelligent Virtual Engineering and the XJTLU Virtual Engineering Center. He completed his PhD in Computer Science from Western University, Canada. Prior to joining XJTLU, he was with the University of Queensland in Australia and the University of Manitoba in Canada. He does research in human–computer interaction, focusing on virtual/augmented reality and gaming technologies.

**Xiaosong Yang** is currently a Professor at the National Centre for Computer Animation, Bournemouth University, UK. He received his bachelor (1993) and master degree (1996) in computer science from Zhejiang University (P. R. China) and PhD (2000) in computing mechanics from Dalian University of Technology (P. R. China). He worked as Post-Doc (2000-2002) in the Department of Computer Science and Technology of Tsinghua University for two years and as Research Assistant (2001-2002) at Chinese University of Hong Kong. His research interests include deep learning, computer vision, computer animation, motion capture & synthesis, VR & AR, special effects & game development, digital health, data mining, medical visualization.

**Jian J. Zhang** is currently a Professor at the National Centre for Computer Animation, Bournemouth University; he leads the Computer Animation Research Centre. His research focuses on a number of topics relating to 3D computer animation, including virtual human modeling and simulation, geometric modeling, motion synthesis, deformation and physics-based animation. He is also interested in virtual reality and medical visualization and simulation. Prof. Zhang has published over 200 peer-reviewed journal and conference publications. He has chaired over 30 international conferences and symposia and serves on a number of editorial boards.